J. Nucl. Phys. Mat. Sci. Rad. A. Vol. 9, No. 1 (2021), pp.61–66

CHITKARA

Journal of Nuclear Physics, Material Sciences, Radiation and Applications

Journal homepage: https://jnp.chitkara.edu.in/

Role of Polar vs Non-polar Configurations in the Decay of $^{268}Sg^{*}$ Compound Nucleus Within the Skyrme Energy Density Formalism

Rajni[1], Kirandeep Sandhu[2*] and M. K. Sharma[3]

[1]*Central University of Jammu, Bagla Suchani, Jammu and Kashmir-181143, India*

[2]*G.S.S.D.G.S Khalsa College, Patiala, Punjab-147001, India*

[3]*Thapar Institute of Engineering and Technology, Patiala, Punjab-147004, India*

[*]kiransndh250@gmail.com (Corresponding Author)

ARTICLE INFORMATION

Received: January 17, 2021
Accepted: April 19, 2021
Published Online: August 31, 2021

Keywords:
Polar and non-polar configuration, Super heavy nuclei, Skyrme forces, Fission cross-section

DOI: 10.15415/jnp.2021.91011

ABSTRACT

The effect of polar and non-polar configurations is investigated in the decay of $^{268}Sg^{*}$ compound nucleus formed via spherical projectile (^{30}Si) and prolate deformed target (^{238}U) using the dynamical cluster decay model. The SSK and GSkI skyrme forces are used to investigate the impact of polar and non-polar (equatorial) configurations on the preformation probability P_0 and consequently on the fission cross-sections of $^{268}Sg^{*}$ nucleus. For non-polar configuration some secondary peaks corresponding to magic shells Z=28 and N=50 are observed, whose magnitude is significantly suppressed for the polar counterpart. The effect of polar and non-polar configurations is further analyzed in reference to barrier lowering parameter ΔV_B. The calculated fission cross-section find adequate agreement with experimental data for chosen set of skyrme forces.

1. Introduction

For the production of super heavy elements the choice of appropriate target projectile combination is extremely important which in-turn leads to cold and hot fusion reactions. In cold fusion reactions, Pb and Bi targets are used at below barrier energies, whereas the use of actinide target leads to hot fusion reactions which take place at relatively higher excitation energies [1-2]. The relatively stable super-heavy nuclear systems are synthesized via highly asymmetric hot fusion reactions where ^{238}U, $^{242,244}Pu$, ^{243}Am, $^{245,248}Cm$, ^{249}Bk and ^{249}Cf actinide targets are collided with the doubly magic ^{48}Ca projectile. Consequently, the hot fusion reactions have been introduced as a tool to understand the dynamics of super-heavy elements and provide a better option for the formation of super heavy systems with $Z \geq 112$.

One of the major factor that influence such reactions is the contribution of the target deformation. The actinide nuclei are generally prolate deformed, so the reaction may proceed either via the equatorial or polar side of the target nucleus. The Coulomb barrier is significantly affected by the orientation and deformation of the interacting nuclei. The effect of orientation is such that, equatorial collision preferred at higher projectile energy results in compound nucleus formation, whereas the polar one leads the non compound nucleus process called quasi-fission. It has been observed that, $^{48}Ca+^{238}U$ [3] and $^{48}Ca+^{242,244}Pu$ [4] reactions have higher fusion probability and measured evaporation residue cross-section are maximum when equatorial configuration is used. The orientation effects on fusion were analyzed for the reaction $^{30}Si+^{238}U$ in ref. [5].

Earlier we had worked on the decay of $^{30}Si+^{238}U$ reaction forming $^{268}Sg^{*}$ compound nucleus [6] using the dynamical cluster-decay model [7-9]. In ref. [6], the role of polar (cold) and non-polar (equatorial) collisions was studied across the Coulomb barrier region using the spin-unsaturated Blocki based potential [10]. At above-barrier energies the calculations were carried out by considering hot-equatorial configuration of nuclei, whereas at sub-barrier energies the cold-polar orientations were included. We had observed significant variations in the mass distribution across the barrier as the fission fragment distribution was symmetric at above barrier energies (for non-polar configurations) and became asymmetric when the nuclei approached pole-to-pole configuration at sub-barrier energies.

As an extension of above work, the present study is carried out where the nuclear potential is obtained from the skyrme energy density formalism (SEDF) [11-12].

ISSN No.: 2321-8649(Print) ISSN No.: 2321-9289(Online); Registration No. : CHAENG/2013/51628

SEDF has contribution from both the spin saturated and spin unsaturated parts of the potential. In this analysis, SSK [13] and GSkI [13] skyrme forces are used which differ significantly in their contribution to the spin. For the study, only below barrier region is chosen and the effect of polar and non-polar configuration and different skyrme forces is inspected. Within the DCM, the decay of ^{30}Si+^{238}U is studied by incorporating the quadrupole deformations of the nuclei along with their optimum orientations of [14].

In order to understand the significance of skyrme forces on the mass distribution the decay of ^{268}Sg* nucleus is studied in terms of preformation probability. It is found that for polar configurations, symmetric fragments show dominance over asymmetric one at lowest incident energies, whereas the asymmetric fragments overtake at higher energies. However in case of non-polar collision, independent of the $E_{c.m.}$, the symmetric fragment show higher magnitude with broader asymmetric peaks. Within both the configurations, the SSK and GSkI skyrme forces are addressed the below barrier fission data.

The paper is organized as follows: the methodology used for the calculation is mentioned in section 2. The calculation and results are discussed in section 3 and finally the summary of the work is presented in section 4.

2. Methodology

2.1. Skyrme Energy Density Formalism (SEDF)

Within SEDF [11-12], the nucleus-nucleus interaction potential is defined as the difference of energy expectation value E of colliding nuclei that are overlapping (at a finite separation distance R) and are completely separated (at $R = \infty$)

$$V_N(R) = E(R) - E(\infty) \tag{1}$$

With E(R) is defined in terms of Hamiltonian density functional H(r)

$$E(R) = \int H(\vec{r})d\vec{r} \tag{2}$$

$$\begin{aligned}
\mathrm{H}(\rho,\tau,\mathrm{J}) = {} & \frac{\hbar^2}{2\mathrm{m}}\tau + \frac{1}{2}\mathrm{t}_0\left[\left(1+\frac{1}{2}\mathrm{x}_0\right)\rho^2 - \left(\mathrm{x}_0+\frac{1}{2}\right)(\rho_\mathrm{n}^2+\rho_\mathrm{p}^2)\right] \\
& + \frac{1}{2}\sum_{\mathrm{i}=1}^{3}\mathrm{t}_{3\mathrm{i}}\rho^{\pm\mathrm{i}}\left[\left(1+\frac{1}{2}\mathrm{x}_{3\mathrm{i}}\right)\rho^2 - \left(\mathrm{x}_{3\mathrm{i}}+\frac{1}{2}\right)\left(\rho_\mathrm{n}^2+\rho_\mathrm{p}^2\right)\right] \\
& + \frac{1}{4}\left[\mathrm{t}_1\left(1+\frac{1}{2}\mathrm{x}_1\right) + \mathrm{t}_2\left(1+\frac{1}{2}\mathrm{x}_2\right)\right]\rho\tau \\
& - \frac{1}{4}\left[\mathrm{t}_1\left(\mathrm{x}_1+\frac{1}{2}\right) - \mathrm{t}_2\left(\mathrm{x}_2+\frac{1}{2}\right)\right]\left(\rho_\mathrm{n}\tau_\mathrm{n}+\rho_\mathrm{p}\tau_\mathrm{p}\right) \\
& + \frac{1}{16}\left[3\mathrm{t}_1\left(1+\frac{1}{2}\mathrm{x}_1\right) - \mathrm{t}_2\left(1+\frac{1}{2}\mathrm{x}_2\right)\right]\left(\vec{\nabla}\rho\right)^2 \\
& - \frac{1}{16}\left[3\mathrm{t}_1\left(\mathrm{x}_1+\frac{1}{2}\right) - \mathrm{t}_2\left(\mathrm{x}_2+\frac{1}{2}\right)\right]\left[\left(\vec{\nabla}\rho_\mathrm{n}\right)^2 + \left(\vec{\nabla}\rho_\mathrm{p}\right)^2\right] \\
& - \frac{1}{2}W_0(\rho\vec{\nabla}.\vec{\mathrm{J}} + \rho_\mathrm{n}\vec{\nabla}.\vec{\mathrm{J}}_\mathrm{n} + \rho_\mathrm{p}\vec{\nabla}.\vec{\mathrm{J}}_\mathrm{p}) \\
& - \left[\frac{1}{16}\left(\mathrm{t}_1\mathrm{x}_1+\mathrm{t}_2\mathrm{x}_2\right)\vec{\mathrm{J}}^2 - \frac{1}{16}\left(\mathrm{t}_1-\mathrm{t}_2\right)\left(\vec{\mathrm{J}}_\mathrm{p}^2+\vec{\mathrm{J}}_\mathrm{n}^2\right)\right].
\end{aligned} \tag{3}$$

Here ρ_q, τ_q and J_q (q=n,p) are the nucleonic, kinetic energy and spin-orbit densities, respectively. m is the nucleon mass. x_i, t_i, α_i, W_0 are the skyrme force parameters, fitted by different authors to obtain better descriptions of various ground state properties of nuclei. In this work GSkI and SSk skyrme forces are used [13].

2.2. Dynamical Cluster Decay Model (DCM)

The dynamical cluster decay model (DCM) [7-9] is a non-statistical approach based on the quantum mechanical fragmentation theory (QMFT). In which all decay modes such as light particle emission (LPs), intermediate mass fragments (IMFs) and fusion-fission (ff) etc are estimated simultaneously in one set of calculation and bring out the nuclear structure information in terms of preformation probability P_0 of decaying fragments. According to DCM, the decay cross-sections in terms of the partial wave analysis is define as:

$$\sigma = \frac{\pi}{k^2}\sum_{\ell=0}^{\ell_{\max}}(2\ell+1)P_0P;\ k = \sqrt{\frac{2\mu E_{c.m}}{\hbar^2}} \tag{4}$$

With μ as the reduced mass, m the nucleon mass and $E_{c.m.}$ the canter of mass energy of the compound nucleus. $\ell_{\max}$ is the maximum angular momentum fixed for the vanishing of the fusion barrier of the incoming channel or the light particle cross section $\sigma_{LP} \to 0$. P_0 is given by the solution of stationary Schrodinger equation in η co-ordinate which reads as:

$$\left\{-\frac{\hbar^2}{2\sqrt{B_{\eta\eta}}}\frac{\partial}{\partial\eta}\frac{1}{\sqrt{B_{\eta\eta}}}\frac{\partial}{\partial\eta} + V_R(\eta,T)\right\}\psi^\nu(\eta) = E^\nu\psi^\nu(\eta) \tag{5}$$

The penetrability P is calculated as the WKB tunneling probability, solved analytically in Ref. [15], as

$$P = \exp\left[-\frac{2}{\hbar}\int_{R_a}^{R_b}\left\{2\mu\left[V(R)-Q_{eff}\right]\right\}^{1/2}dR\right]$$

Table 1: The fission cross-sections for the decay of ^{286}106 compound nucleus calculated using SSK and GSkI skyrme forces along with their respective angular momentum (ℓ) values. The table shows the result of non-polar configuration.

$E_{c.m.}$ (MeV)	T (MeV)	σ_{DCM} (mb)		σ_{expt} (mb)	ℓ ($\hbar$)	
		GSkI	SSK		GSkI	SSK
125	1.154	0.122	0.120	0.123	79	75
129	1.225	3.72	3.74	3.25	86	83
134	1.307	20.8	20.8	20.0	94	90

with $V(R_a,T) = V(R_b,T) = \mathrm{TKE}(T) = Q_{\mathrm{eff}}$ for the entry and exit points of the potential barrier. Q_{eff} is the effective Q value of the decay process and the entry point $R_a = R_1(\alpha_1,T) + R_2(\alpha_2,T) + \Delta R(\eta,T) = R_t(\alpha_i,T) + \Delta R(\eta,T)$. In above equation, α_i (i = 1, 2) is an angle that the radius vector R_i of the colliding nuclei makes with the symmetry axis, measured clockwise. ΔR refers to the neck-length parameter which assimilates the neck formation effects. The choice of ΔR for a best fit to the data allows us to define the effective "barrier lowering" parameter $\Delta V_B(\ell)$ as [8]

$$\Delta V_B(\ell) = V(R_a,\ell) - V_B(\ell) \tag{6}$$

The deformation and orientation dependent fragmentation potential V(R) at any temperature is given as

$$\begin{aligned} V_R(\eta,T) = &\sum_{i=1}^{2}\left[V_{LDM}(A_i,Z_i,T)\right] \\ &+\sum_{i=1}^{2}\left[\delta U_i\right]\exp(-T^2/T_0^2) + V_c(R,Z_i,\beta_{\lambda i},\theta_i,T) \\ &+V_N(R,A_i,\beta_{\lambda i},\theta_i,T) + V_\ell(R,A_i,\beta_{\lambda i},\theta_i,T) \end{aligned} \tag{7}$$

where the T-dependent terms V_C, V_N and V_ℓ are defined as follows: V_c is the Coulomb potential, V_N is the nuclear potential for hot deformed nuclei, and V_ℓ is the potential due to rotational motion of hot deformed nuclei. In this work V_N is calculated using the skyrme energy density formalism explained briefly in section 2.1.

3. Calculation and Result

In this section, we investigate the decay of ^{268}Sg* compound nucleus within the center-of-mass energies $E_{c.m.}$ = 125–134 MeV (below barrier region) using polar and non-polar configurations of the colliding nuclei. For the study, the SEDF approach with two skyrme forces such as SSK and GSkI are applied to understand the fusion-fission dynamics of the ^{30}Si+^{238}U→^{268}Sg* reaction. The result related to preformation probability (P_0) and the barrier modification parameters (ΔV_B) are outlined in the present work.

Fig. 1 shows the variation of preformation probability (P_0) as a function of fragment mass (A_i) for the decay of ^{286}Sg* compound nucleus. Left and right panels respectively illustrate the result for non-polar and polar configurations using GSkI and SSk skyrme forces. The graph is plotted for below barrier center of mass energies i.e. $E_{c.m.}$=125 MeV to 134 MeV. On comparing the non-polar and polar configurations at same center of mass energy i.e. at $E_{c.m.}$=125 MeV, we observe the following:

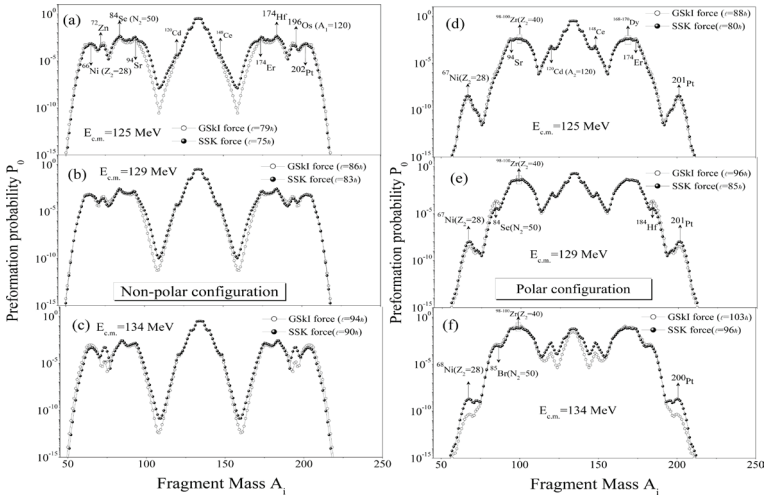

Figure 1: Left and right panels show the variation of Preformation probability P_0 as a function of fragment mass (A_i) plotted for the decay of ^{286}Sg* compound nucleus respectively for non-polar and polar configurations. The graph demonstrate the calculation of GSkI and SSK skyrme forces. The below barrier center of mass energies $E_{c.m.}$ for the compound nucleus is also mentioned in the figure.

(i) for non-polar approach, both symmetric and asymmetric peaks are visible; although the probability of symmetric fission is higher than the asymmetric one. In asymmetric fission region significant contribution from the secondary peaks at ^{66}Ni, ^{72}Zn and ^{84}Se (and their complementary fragments) are also observed, which corresponds to the shell closure at Z_2=28, Z_2=40 and N_2=50. Hence the role of the magic shell closures play significant role in the decay dynamics of ^{268}Sg* nucleus.

Table 2: Same as "Table 1" but results are shown for Polar configuration.

$E_{c.m.}$ (MeV)	T (MeV)	σ_{DCM} (mb)		$\sigma_{expt.}$ (mb)	ℓ ($\hbar$)	
		GSkI	SSK		GSkI	SSK
125	1.154	0.190	0.142	0.123	88	80
129	1.225	3.08	3.94	3.25	96	85
134	1.307	21.40	20.4	20.0	103	96

(ii) On the other hand, when polar configuration is applied, the magnitude of the secondary peak around ^{66}Ni decreases at the cost of enhanced magnitude of preformation probability at deformed magic shell around Z=40 (isotope of $^{98\text{-}100}$Zr) as shown in Fig.1(d). It is to be noted here that, above result is true for either choice of the skyrme forces.

Further Fig. 1(a) to (c) shows that, when center of mass energy increases from 125 to 134 MeV, similar fragments are formed for non-polar approach. However in polar configuration, the fragment mass distribution of decaying fragments changes significantly with increase in incident energy. While looking at Fig. 1(d) to 1(f), it is observed that with increase in energy, the probability of symmetric fission decreases and an asymmetric peak around ^{84}Se (N_2=50) starts appearing. Thus we find that, the decay pattern of compound nucleus ^{286}Sg* is greatly influenced by the orientational configuration and the incident energy.

We have addressed the fission cross-sections of ^{286}Sg* compound nucleus within both the configuration and using SSK and GSkI skyrme forces. "Table 1" and "Table 2" illustrate the DCM calculated fission cross-sections, angular momentum values (ℓ) and center of mass energy ($E_{c.m.}$) along with the experimentally given data.

Fig. 2(a) and Fig. 2(b) depict the fitting parameter 'ΔR' as a function of $E_{c.m.}$ plotted with GSkI and SSK forces. We observe in Fig. 2(a) that, independent of the configuration, ΔR increases with increase in $E_{c.m.}$.

It is to be observed that, in non-polar approach higher neck length is required to fit the fission data (as compared to polar configuration). Similar results are obtained when SSK force is used (as shown in Fig. 2(b)).

For sub-barrier energies, barrier modification parameter ΔV_B is a crucial factor, has a direct dependence on the corresponding values of neck-length ΔR (see equation (6) of section 2) used to address the fission data. Fig. 3 shows the variation of ΔV_B with center of mass energy $E_{c.m.}$ plotted for non-polar and polar configuration. From Fig. 3(a) one may observe that, using GSkI force, larger modification in barrier is required for non-polar configuration in comparison to polar configuration. Similar observations are drawn with SSk skyrme force.

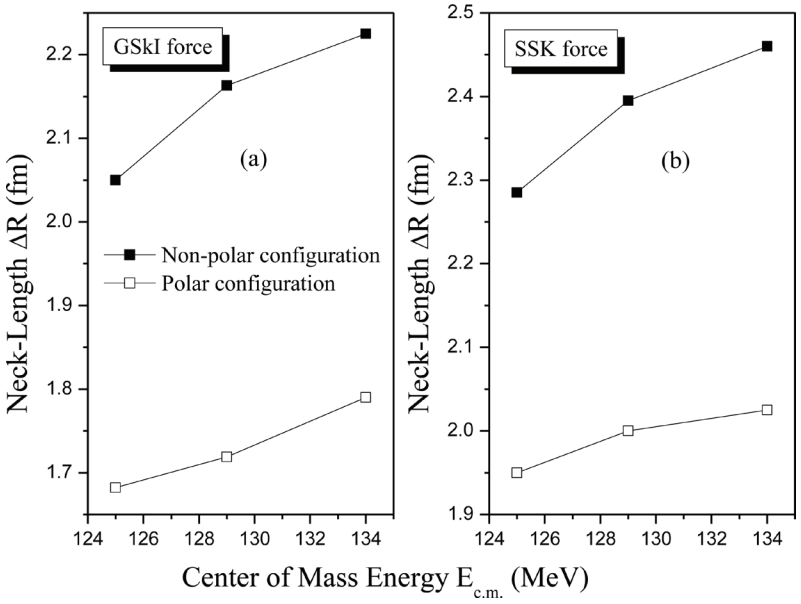

Figure 2: Variation of neck length ΔR as a function of $E_{c.m}$ for non-polar and polar configuration plotted with (a) for GSkI force and (b) for SSK force.

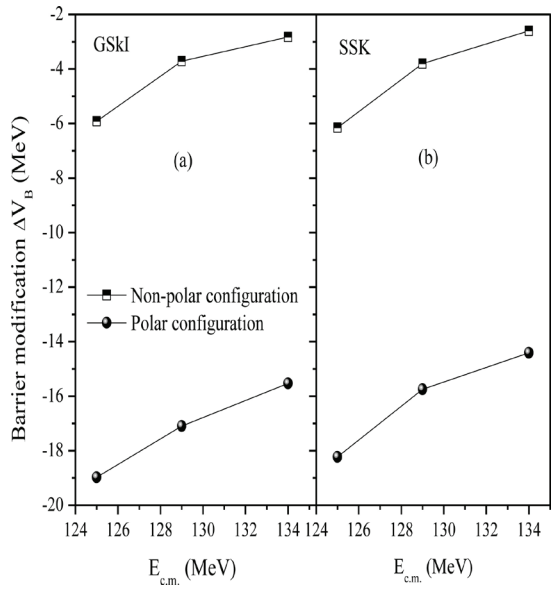

Figure 3: The barrier-lowering parameter ΔV_B as a function of $E_{c.m.}$ for the decay of $^{268}Sg^*$ to most probable fragment for (a) GSkI force and (b) for SSk force at $\ell=\ell_{max.}$

Summary

The purpose of this work is to investigate the role of polar and non-polar configurations on the fission dynamics of $^{268}Sg^*$ compound nucleus at below the Coulomb barrier energy. The study is carried out by estimating the preformation probability P_0 and fission cross-sections within the framework of dynamical cluster decay model. It is to be observed that, within the scope of skyrme based nuclear potential, the probability of asymmetric fragments increases with increase in the preformation energy when nuclei interacted via pole to pole, which on the other hand remains the unchanged for the case of non-polar interactions. This result is independent of the skyrme force used. The addressal of experimental data within the non-polar orientation demands higher value of neck-length parameter ΔR and consequently larger barrier modification as compared to the polar configuration.

Acknowledgement

One of us is thankful for the financial assistance in terms of minor project (Letter No. KCP/2020/MS/2186-2191), available from the G.S.S.D.G.S Khalsa College Research Fund.

References

[1] S. Hofmann and G. M¨unzenberg, Rev. Mod. Phys. **72**, 733 (2000). https://doi.org/10.1103/RevModPhys.72.733

[2] K. Morita et al., J. Phys. Soc. Jpn. **73**, 1738 (2004). https://doi.org/10.1143/JPSJ.73.2593

[3] Y. Oganessian, J. Phys. G **34**, R165 (2007). https://doi.org/10.1088/0954-3899/34/4/R01

[4] Yu. Ts. Oganessian et al., Phys. Rev. C **70**, 064609 (2004). https://doi.org/10.1103/PhysRevC.70.064609

[5] K. Nishio et al., Eur. Phys. J. A **29**, 281 (2006). https://doi.org/10.1140/epja/i2006-10091-y

[6] K. Sandhu, M. K. Sharma and R. K. Gupta, Phys. Rev. C **86**, 064611 (2012). https://doi.org/10.1103/PhysRevC.86.064611

[7] M. Kaur, R. Kumar and M. K. Sharma, Phys. Rev. C **85**, 014609 (2012). https://doi.org/10.1103/PhysRevC.85.014609

[8] Rajni, R. Kumar and M. K. Sharma Phys. Rev. C **90**, 044604 (2014). https://doi.org/10.1103/PhysRevC.90.044604

[9] G. Kaur, K. Sandhu and M. K. Sharma, Nucl. Phys. A **971**, 95 (2018). https://doi.org/10.1016/j.nuclphysa.2018.01.017

[10] J. Blocki, J. Randrup, W. J. Swiatecki and C. F. Tsang, Ann. Phys. (NY) **105**, 427 (1977). https://doi.org/10.1016/0003-4916(77)90249-4

[11] D. Vautherin, Phys. Rev. C **7**, 296 (1973). https://doi.org/10.1103/PhysRevC.7.296

[12] Rajni, D. jain, I. Sharma and M. K. Sharma, Eur. Phys. J A **53**, 208 (2017). https://doi.org/10.1140/epja/i2017-12407-2

[13] B. K. Agrawal, S. K. Dhiman and R. Kumar, Phys. Rev. C **73**, 034319 (2006). https://doi.org/10.1103/PhysRevC.73.034319

[14] R. K. Gupta et al., J. Phys. G: Nucl. Part. Phys. **31**, 631 (2005). https://doi.org/10.1088/0954-3899/31/7/009

[15] G. Wentzel, Z. Phys. **38**, 518 (1926). https://doi.org/10.1007/BF01397171

H. A. Kramers, Z. Phys. **39**, 828 (1926). https://doi.org/10.1007/BF01451751

Journal of Nuclear Physics, Material Sciences, Radiation and Applications

Chitkara University, Saraswati Kendra, SCO 160-161, Sector 9-C, Chandigarh, 160009, India

Volume 9, Issue 1 **August 2021** **ISSN 2321-8649**